INSTABILITY OF THE IONOSPHERIC PLASMA: MODELING AND ANALYSIS *

CHRISTOPHE BESSE†, JEAN CLAUDEL‡, PIERRE DEGOND§, FABRICE DELUZET¶, GÉRARD GALLICE‖, AND CHRISTIAN TESSIERAS**

Abstract. This paper is concerned with the theory and modeling of plasma instabilities in the ionosphere. We first consider the so-called 'striation model' which consists of balance equations for the density and momenta of the plasma species, coupled with an elliptic equation for the potential. The linearized instability of this model is analyzed in the framework of Fourier theory, both for smooth and discontinuous steady-states. Then, we show that the dissipation mechanisms at work in the more refined 'dynamo model' allow to stabilize high wave-number perturbations. We also analyze turbulence as a possible source of additional dissipation (in a similar way as in fluid mechanics). To this aim, we use the statistical approach to turbulence and derive a so-called 'turbulent striation model', of which we analyze the stability properties. Numerical experiments are used to support our investigations.

Key words. Euler-Maxwell system, dynamo model, striation model, ionospheric plasma, striations, turbulence, statistical approach, linearized stability analysis

AMS subject classifications. 82D10, 76N99, 76X05, 76W06, 78M35

1. Introduction.

This paper is concerned with the modeling and analysis of plasma instabilities in the ionosphere, at altitudes ranging between a few hundred and a thousand kilometers (F region). The plasma may be created, either by the natural ionization of the atmosphere, or by possible artificial causes (such as e.g. thermonuclear explosions [29], [41], [17]). The ionospheric plasma is strongly structured by the earth magnetic field. Indeed, the mobility of the ionized species (i.e. their velocity in response to an external electric field) is strongly anisotropic: while field-aligned mobilities (i.e. mobilities in the direction of the magnetic field) are large, transverse mobilities (also called Pedersen mobilities) are quite small. Additionally, a component of the plasma velocity orthogonal to both the electric and magnetic fields appears as a result of the Hall effect. This component is the major actor in the so-called $E \times B$ drift instability which we are going to discuss in the present paper.

At lower altitudes, the density of the neutral atmosphere is large and the plasma is dragged by the motion of the neutral molecules (or neutral wind). As a result, a net electrical current flows across the magnetic field lines and generates an induced electric field. This is the so-called ionospheric dynamo effect [1]. The reader car refer to [35], [19], [7] and [2] for reviews about ionospheric physics. In the presence of a gradient in the plasma density, the neutral wind can trigger the $E \times B$ drift instability, which bears strong analogies with the Rayleigh-Taylor instability in fluid mechanics [8]. This instability produces strong inhomogeneities (the ionospheric striations) which soon

*Supports by the 'Centre d'Etudes Scientifiques d'Aquitaine' of the 'Commisariat à l'Energie Atomique' and by the European network HYKE, funded by the EC as contract HPRN-CT-2002-00282 are gratefully acknowledged.

†Mathématiques pour l'Industrie et la Physique, CNRS UMR 5640, Université Paul Sabatier, 118 Route de Narbonne, 31062 Toulouse Cedex 4, France (besse@mip.ups-tlse.fr).

‡Commissariat à l'Energie Atomique, Centre d'Etudes Scientifiques et Techniques d'Aquitaine, BP2, 33114 Le Barp, France (Jean.Claudel@cea.fr).

§Mathématiques pour l'Industrie et la Physique (degond@mip.ups-tlse.fr).

¶Mathématiques pour l'Industrie et la Physique (deluzet@mip.ups-tlse.fr).

‖Commissariat à l'Energie Atomique (Gerard.Gallice@cea.fr).

**Commissariat à l'Energie Atomique (Christian.Tessieras@cea.fr).

propagate over hundreds of kilometers along the magnetic field lines. The generation of plasma irregularities is reviewed in [11], [12], [34].

Our goal is to discuss some aspects of the mathematical and numerical modeling of this instability. Striations as well as related instability phenomena of the ionospheric plasma have been the subject of a wide literature (see e.g. discussions of the 'Spread F' in [42], [24], [32], of the equatorial electrojet in [6], [39], [36], [37] and of Baryum releases experiments in [10]). The well-accepted mathematical model for these phenomena is the 'dynamo' model [42], [10] which consists of mass and momentum balance equations for the plasma species. A simpler model, the 'striation' model, is obtained when the field-aligned mobilities are supposed infinite. The derivation of these models and their interrelations are reviewed in [3], and will be briefly recalled in section 2.

The $E\times B$ drift instability is well-described in the framework of the striation model (see section 3). A linear stability analysis indeed shows that exponential density profiles are unstable (see the review in [12] and section 3.2). Exponential density profiles are the only non-constant smooth stationary states which allow analytical computations (via Fourier analysis). However, they are quite unrealistic and a better theory should consider discontinuous density profiles. We consider this problem in section 3.3 and show that the striation model is also unstable in this case for certain configurations of the neutral wind. In a companion work [5], we show that smooth density profiles which are linearly unstable are nonlinearly unstable. However, the proof of [5] does not extend to discontinuous solutions. Similarly, we do not know, even for smooth density profiles, if linear stability implies nonlinear stability.

In practice, the instability saturates and cascades towards smaller scales by nonlinearity [11], [37], [39], [23], [31], untill it is ultimately damped by dissipation. In the striation model however, all dissipation mechanisms have been removed. In section 4, we reintroduce dissipation effects by considering the dynamo model, where both finite temperature and finite conductivity effects are retained. A linearized stability analysis shows that high wave-number perturbations are damped. However, in practice, the magnitude of the dissipation is too small and we must consider other sources of dissipation.

In this paper, we investigate the possible influence of fluid turbulence. In fluid mechanics, it is a well-known fact that turbulence may enhance dissipation ([30] and references therein). The statistical approach to fluid turbulence considers averages of the Navier-Stokes equations over various approximate realizations of the same solution. The chains of resulting statistical equations are closed by various types of phenomenological assumptions which are still mathematically unjustified except in very simple cases, such as that considered in [25]. The obtained models (such as the K-ϵ model) involve additional terms compared with the standard Navier-Stokes equations which describe the enhancement of diffusion by turbulence.

In section 5, we develop a similar statistical framework to model turbulence within the striation model (see also [26] for an application to MHD theory). We first derive an averaged striation model, for which we propose a closure Ansatz inspired by [25]. This leads to a diffusive version of the striation model, the 'turbulent striation model'. To find the value of the turbulent diffusion constant, a stability analysis of the model is performed. It allows to relate the threshold wave-number for instability (i.e. the typical size of the finest persisting structures in the plasma, which can be experimentally observed) with the value of this constant.

Section 6 is devoted to numerical simulations. Their goal is to provide a numerical

and quantitative evidence of the features predicted in section 5, namely that the turbulent striation model produces persisting structures whose typical size is related to the magnitude of the diffusion.

Turbulence modeling in ionospheric plasmas has been widely investigated in the literature. Most of the approaches rely on nonlinear Fourier analysis [37], [20], [21] and bear similarities with the spectral approach to turbulence in fluid mechanics [27] (see also [13] for applications of these ideas to other plasma physics contexts). In using the statistical approach, we have chosen a slightly different route.

2. The 'dynamo' and 'striation' models of the ionospheric plasma. We consider two different species of particles: electrons and one ion species. They are assumed so dilute that they have no influence on the dynamics of the neutrals, the velocity of which $u_n(x,t)$ (also called the neutral wind) is supposed known. In [3], a hierarchy of models for the ionospheric plasma has been derived. Of particular interest in the present study are the 'dynamo' and 'striation' models. The dynamo model is written as follows:

$$\partial_t n + \nabla \cdot (n u_i) = 0\,, \tag{2.1}$$

$$-\nabla\phi + u_{e,i} \times B = \kappa q_{e,i} \left[\nu_{e,i}(u_{e,i} - u_n) + \eta \nabla \log n\right]\,. \tag{2.2}$$

$$\nabla \cdot j = 0\,, \quad \kappa j = n(u_i - u_e)\,, \tag{2.3}$$

where we denote by $n(x,t)$ the density of the plasma, $u_e(x,t)$, $u_i(x,t)$, the electron and ion velocities, $j(x,t)$ the plasma current, $\phi(x,t)$, the electric potential, $B(x)$, the earth magnetic field and $\nu_e(x)$, $\nu_i(x)$, the electron-neutral and ion-neutral collision frequencies. These quantities depend on the 3-dimensional position coordinate x and on the time $t \geq 0$. The parameters η and κ are dimensionless and defined below. Eq. (2.2) actually consists of two equations, one for the electrons (with the index 'e' chosen everywhere) and one for the ions (with the index 'i'). We let $q_i = 1$, $q_e = -1$. We suppose that the geomagnetic field $B(x)$ is unperturbed by the presence of the plasma and is known. Similarly, the collision frequencies $\nu_e(x)$, $\nu_i(x)$, which primarily depend on the neutral density, are supposed known. The plasma is supposed quasi-neutral, i.e. the electron and ion densities coincide with n. Despite the quasi-neutrality, the electron and ion velocities can be different, giving rise to a non-zero plasma current j. We have also supposed that the electron and ion gases are isothermal with the same uniform temperature.

System (2.1)-(2.3) is written in dimensionless units. The scaling units and their typical values in the situations of interest are summarized in table 2.1 below. The parameters η and κ are given by:

$$\eta = \frac{k_B \bar{T}}{m_i \bar{u}^2} \frac{1}{\bar{\nu}_i \bar{t}}\,, \quad \kappa = \frac{m_e \bar{\nu}_e}{e\bar{B}} = \frac{m_i \bar{\nu}_i}{e\bar{B}}\,,$$

(where k_B is the Boltzmann constant) and respectively measure the ratio of the thermal energy to the ion drift energy and the typical number of electron-neutral or ion-neutral collisions per rotation period in the geomagnetic field. These two parameters have typical values (according to table 2.1):

$$\eta \sim 10^1\,, \quad \kappa \sim 10^{-4}\,. \tag{2.4}$$

Since κ is small, it is meaningful to investigate the limit of the dynamo model when $\kappa \to 0$. This leads to the so-called striation model that we give in more detail below.

Quantity	Scaling unit	Value
Time	$\bar{t}$	10^3 s
Length	$\bar{x}$	10^5 m
Velocity	$\bar{u} = \bar{x}/\bar{t}$	10^2 ms^{-1}
Density	$\bar{n}$	10^{12} m^{-3}
Temperature	$\bar{T}$	10^3 K
Magnetic field	$\bar{B}$	10^{-5} T
Electric potential	$\bar{\phi} = \bar{u}\bar{B}\bar{x}$	10^2 V
e-n collision frequency	$\bar{\nu}_e$	10^2 s^{-1}
i-n collision frequency	$\bar{\nu}_i = \frac{m_e}{m_i}\bar{\nu}_e$	10^{-2} s^{-1}

TABLE 2.1
Scaling units

Before doing so, we rewrite the dynamo model in a more appropriate form. In a local reference frame in which the last basis vector is aligned with the magnetic field, the ion and electron mobility matrices $\mathbb{M}_e$ and $\mathbb{M}_i$ are given by:

$$\mathbb{M}_e = \begin{pmatrix} \mu_e^P & -\mu_e^H & 0 \\ \mu_e^H & \mu_e^P & 0 \\ 0 & 0 & \mu_e^\parallel \end{pmatrix}, \quad \mathbb{M}_i = \begin{pmatrix} \mu_i^P & \mu_i^H & 0 \\ -\mu_i^H & \mu_i^P & 0 \\ 0 & 0 & \mu_i^\parallel \end{pmatrix},$$

where the electron and ion Pedersen, Hall and field-aligned mobilities are respectively defined by

$$\mu_{e,i}^P = \frac{\kappa\nu_{e,i}}{(\kappa\nu_{e,i})^2 + |B|^2}, \quad \mu_{e,i}^H = \frac{|B|}{(\kappa\nu_{e,i})^2 + |B|^2}, \quad \mu_{e,i}^\parallel = \frac{1}{\kappa\nu_{e,i}}.$$

In the situation $\kappa \to 0$, the electron or ion field-aligned mobilities tend to infinity.

Thanks to the mobility matrices, equations (2.2) and (2.3) may be rewritten as

$$u_{e,i} = \mathbb{M}_{e,i}\left(-q_{e,i}\nabla\phi + \kappa(\nu_{e,i}u_n - \eta\nabla\log n)\right), \tag{2.5}$$

$$-\nabla\cdot(n(\mathbb{M}_i + \mathbb{M}_e)\nabla\phi)) = \\ = -\kappa\nabla\cdot(n[\mathbb{M}_i(\nu_i u_n - \eta\nabla\log n) - \mathbb{M}_e(\nu_e u_n - \eta\nabla\log n)]). \tag{2.6}$$

It is clear that the conductivity matrix $n(\mathbb{M}_i + \mathbb{M}_e)$ is positive definite (provided that ν_i or ν_e is positive and finite). Therefore, (2.6) is a three-dimensional elliptic equation for ϕ.

Now, we assume that the magnetic field is constant and uniform (see [3] and [4] for an extension to the non-uniform B case). Let us denote by $(\hat{x}_1, \hat{x}_2, \hat{x}_3)$ the orthonormal coordinate basis, with $\hat{x}_3$ aligned with B. We can choose the scaling units such that $|B| = 1$, so that $B = \hat{x}_3$. We denote by $\underline{x} = (x_1, x_2)$ the position vector in the 2-dimensional plane orthogonal to B and $\underline{\nabla} = (\partial_{x_1}, \partial_{x_2})$ the 2-dimensional gradient. For any 3-dimensional vector $a = (a_1, a_2, a_3)$, we define $\underline{a} = (a_1, a_2)$ its projection onto this plane.

When $\kappa \to 0$, the dynamo model reduces to the the so-called striation model [3]:

$$\partial_t n + \nabla\cdot(nu) = 0, \tag{2.7}$$

$$u = -\underline{\nabla}\phi \times B + ((u_n - \eta\nu^{-1}\nabla\log n)\cdot B)B, \tag{2.8}$$

$$\underline{\nabla}\cdot((-\sigma(\underline{x})\underline{\nabla}\phi + (U_n - 2\eta\underline{\nabla}N)\times B) = 0, \tag{2.9}$$

with $\phi = \phi(\underline{x})$, $\sigma(\underline{x}) = \int n\nu dx_3$, $U_n = \int n\nu u_n dx_3$, $N = \int n dx_3$, $\nu = \nu_i + \nu_e$ and $u_i = u_e = u$. The striation model couples a 3-dimensional convection-diffusion equation (2.7), (2.8) for the density n with a 2-dimensional elliptic equation (2.9) for the electric potential ϕ. The coefficients of the elliptic equation (2.9) involve integrals of n over x_3 i.e. along the magnetic field lines. The infinite conductivity of the plasma along the magnetic field lines constrains the electric potential to be constant along these lines, i.e. to depend only on the 2-dimensional coordinate $\underline{x}$.

If we additionally suppose that u_n is orthogonal to B and that all data and unknowns are independent of x_3, the striation model reduces to the following monolayer striation model:

$$\partial_t n + \nabla \cdot (nu) = 0\,, \quad u = -\nabla\phi \times B\,, \tag{2.10}$$

$$\nabla \cdot (nh) = 0\,, \quad h = \nu\left(-\nabla\phi + (u_n - 2\eta\nu^{-1}\nabla \log n) \times B\right)\,, \tag{2.11}$$

where now, all variables and vectors are 2-dimensional (except $B = \hat{x}_3$) and the underlying of 2-dimensional vectors has been omitted. The quantity h represents the electron-ion relative velocity. We remark that $\nabla \cdot u = 0$. Therefore, we can write relation (2.10)

$$\partial_t n + (u \cdot \nabla)n = 0\,. \tag{2.12}$$

As we will next see, the pressure term $\nabla \log n$ does not change the linearized stability properties of the striation model. When $\eta = 0$, (2.11) becomes:

$$\nabla \cdot (nh) = 0\,, \quad h = \nu\left(-\nabla\phi + u_n \times B\right). \tag{2.13}$$

In the next section, we analyze the linearized stability of this model.

3. Stability analysis of the striation model.

3.1. Introduction and phenomenology. The striation model exhibits an instability, the gradient-drift or $E \times B$ drift instability [11], [12]. In a recent work [5], local-in-time existence and uniqueness of solutions for this model have been proven and, following the methodology of [16], [18], [9], [22] smooth stationary density profiles which are linearly unstable have been shown to be non-linearly unstable. However, it is still open whether the converse is true. In [5], a variational formulation for the instability growth rate is given. In the present work, we are aiming at a more quantitative result for certain specific classes of stationary profiles.

We restrict to two particular kinds of steady-state profiles. The first ones are smooth with an exponentially increasing density in one direction; they have already been investigated [11], [12] and we shall only summarize the results. The second ones are discontinuous density profiles; their analysis is, to the best of our knowledge, new. In passing, we shall have to show that it is meaningful to consider discontinuous solutions of the striation model.

We first give a phenomenological view of the instability of the striation model. We consider a steady state consisting of a discontinuous density $n(x) = \underline{n}$ for $x_2 < 0$ and $n = \overline{n} > \underline{n}$ for $x_2 > 0$, with $\nabla\phi = 0$ and $u_n = (0, U)$. We slightly perturb the interface which is now represented by the graph of the function $x_2 = \varepsilon \sin(\xi x_1)$ where ε represents the magnitude of the perturbation ($\varepsilon \ll 1$) and ξ is its spatial frequency.

The term $u_n \times B$ in (2.13) creates a charge modulation along the interface which is alternately positive and negative. A non-zero electric field $-\nabla\phi$ parallel to the interface with a similar sign modulation is generated according to (2.13). Then, by

(2.10) a non-zero component of the velocity u in the direction normal to the interface is created with again an alternating sign. According to the sign of u_n, this component of the velocity tends to either damp the modulation of the interface or increase it. The former case is a stable one while the latter is an unstable one. The precise geometric configuration is depicted on figure 3.2.

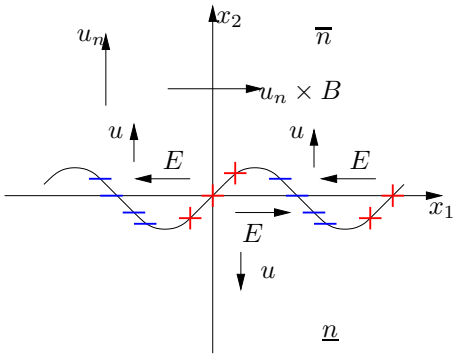

FIG. 3.1. *Stable configuration*

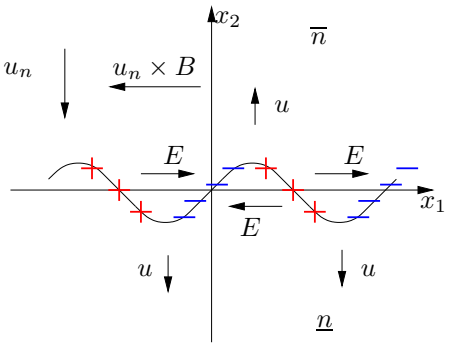

FIG. 3.2. *Unstable configuration*

This behavior can be recovered by the linear stability analysis. We first turn to the analysis of the exponential density profile. In the remainder of this section, we assume that ν is a uniform constant and by a convenient choice of the scaling units, we let $\nu = 1$.

3.2. Linear stability analysis : the exponential density profile . Let us denote by (n^0, u^0, h^0, ϕ^0) the unperturbed state, i.e. a time-independent solution of the striation system (2.10), (2.13). We consider an exponential density profile in the x_2-direction, i.e. $n^0 = N\exp(x_2/\lambda)$, where $\lambda > 0$ is the gradient length, while $(u^0, h^0, \nabla\phi^0)$ are uniform constants. We suppose that the neutral wind is uniform as well and has components $u_n = (V, U)$. In this configuration, a necessary and sufficient condition for (n^0, u^0, h^0, ϕ^0) to form a steady-state is that $u^0 = (V, 0)$, $h^0 = (\nu U, 0)$, $-\nabla\phi^0 = (0, V)$. In this analysis, we suppose that $\eta = 0$, unless otherwise specified.

Then, we introduce the perturbation $n = n^0(1 + \varepsilon n^1 + O(\varepsilon^2))$, $(u, h, \phi) = (u^0, h^0, \phi^0) + \varepsilon(u^1, h^1, \phi^1) + O(\varepsilon^2)$, with $\varepsilon \ll 1$ in the striation model and neglect the terms of order higher than ε. The neutral wind being a datum remains unperturbed. We note that $\nabla n^0 = (0, n^0/\lambda)$. An easy computation gives the linearized system governing the first order perturbation:

$$\partial_t n^1 + \lambda^{-1}\partial_{x_1}\phi^1 + V\partial_{x_1} n^1 = 0\,, \tag{3.1}$$

$$-\lambda^{-1}\partial_{x_2}\phi^1 - \Delta\phi^1 + U\partial_{x_1} n^1 = 0\,, \tag{3.2}$$

REMARK 3.1. *If the pressure gradient terms are retained in the model (i.e. if $\eta \neq 0$), the steady-state is only modified through the expression of h^0 which should be taken as $h^0 = (U - 2\eta\lambda^{-1}, 0)$. However, the first order perturbation equations are the same as (3.1), (3.2). The details are left to the reader.*

We develop the solution of (3.1), (3.2) into plane waves, i.e. (dropping the superscripts '1' for clarity) $(n, \phi) = (\bar{n}, \bar{\phi}\lambda|U|)\exp\left(i\lambda^{-1}\left(\xi_1 x_1 + \xi_2 x_2 - \omega t|U|\right)\right)$ where $\xi = (\xi_1, \xi_2)$ is the (normalized) wave-vector of the perturbation and ω its frequency. Introducing this Ansatz into (3.1), (3.2), we get:

$$-\omega\bar{n} + \xi_1\bar{\phi} = 0\ ; \quad i\sigma\xi_1\bar{n} + (\xi_1^2 + \xi_2^2 - i\xi_2)\bar{\phi} = 0\,, \tag{3.3}$$

with $\sigma = \text{sign}(U) \in \{-1, 1\}$. This system has a non trivial solution iff its determinant is non vanishing. This condition yields the dispersion relation

$$\omega = \frac{-i\sigma\xi_1^2}{(\xi_1^2+\xi_2^2)^2+\xi_2^2}(\xi_1^2+\xi_2^2+i\xi_2)\,, \tag{3.4}$$

We now recall the following standard

DEFINITION 3.2. *The perturbation is stable if n and ϕ stay bounded for all times $t \geq 0$ and unstable in the converse situation. Therefore, a perturbation is stable iff $\Im m(\omega) \leq 0$ and unstable iff $\Im m(\omega) > 0$ A stationary state is called stable if all its perturbations are stable for all wave vectors ξ. It is unstable as soon as there exists a wave vector ξ giving rise to an unstable perturbation.*

Thanks to (3.4), we have $\text{sign}(\Im m(\omega)) = -\sigma$. It follows:

PROPOSITION 3.3. *The steady-state configuration with an exponential density profile is stable if and only if $U \geq 0$, i.e. if the x_2-component of the neutral wind points in the same direction as the density gradient. Furthermore, in the case $U < 0$, all wave vectors $\xi \neq 0$ are unstable and for $\xi_2 = 0$ the growth rate is independent of ξ_1.*

As seen above, exponential density profiles allow explicit computations. However, they are fairly unrealistic, as the density tends to infinity on one side and degenerates to zero (and the elliptic problem (2.13) as well) on the other side. In order to study a more realistic situation, we extend our analysis to the case of a discontinuous density profiles in the next section.

3.3. Linear stability analysis : discontinuous density profiles. We consider a density profile which is piecewise constant and discontinuous across a parametrized curve $C(t)$ given by the equation $x_2 = f(x_1, t)$, where $f \in C^1(\mathbb{R} \times [0, +\infty[)$ i.e.

$$n(x,t) = \begin{cases} \underline{n} & \text{for} \quad x_2 < f(x_1,t)\,, \\ \overline{n} & \text{for} \quad x_2 > f(x_1,t)\,. \end{cases} \tag{3.5}$$

First, we must give a meaning to discontinuous solutions of this kind. To this aim, we use the notion of weak solution of (2.12).

DEFINITION 3.4. *let $u \in C^1(\mathbb{R}^2 \times [0,\infty[)$. A function $n \in L^\infty_{loc}(\mathbb{R}^2 \times [0,\infty))$ is a weak solution of (2.12) with initial data n_0 if and only if n verifies*

$$\int_{\mathbb{R}^2\times[0,\infty)} n\left(\frac{\partial\varphi}{\partial t} + \nabla\cdot(u\varphi)\right) dx\,dt + \int_{\mathbb{R}^2} n_0\,\varphi(x,0)\,dx = 0\,, \tag{3.6}$$

for all functions $\varphi(x,y,t) \in C^1_c(\mathbb{R}^2 \times [0,\infty))$, where C^1_c defines the space of functions of class C^1 with compact support.

The solution of (3.6) can be obtained through the method of characteristics. In particular, it satisfies the maximum principle. Therefore, if there exist two constants n_*, n^* such that $0 < n_* < n_0(x) < n^*$, this inequality is satisfied at all times: $0 < n_* < n(x,t) < n^*$.

This notion has to be extended to the case of discontinuous velocities. Suppose that $u = (u_1, u_2)$ is taken in the space $L^1_{\text{loc}}([0,\infty), H_{\text{div}})$, with $H_{\text{div}}(\mathbb{R}^2) = \{u \in L^2(\mathbb{R}^2)$, s.t. $\nabla\cdot u \in L^2(\mathbb{R}^2)\}$. Then, $\nabla\cdot(u\varphi) \in L^1_{\text{loc}}(\mathbb{R}^2\times[0,\infty))$ for all test functions φ and the expression (3.6) still has a meaning. Now, in the striation model, u is a given by $u = -\nabla\phi \times B$ where ϕ is a solution of (2.13). To solve (2.13), we use the following (classical) proposition:

PROPOSITION 3.5. *Let $u_n \in L^2(\mathbb{R}^2)$ and n be such that there exist two constants n_*, n^* with $0 < n_* < n(x,t) < n^*$. Then, eq. (2.13), which can be written*

$$\nabla \cdot (n \nabla \phi) = \nabla \cdot (n u_n \times B)\,,$$

has a solution in the space $L^1_{loc}([0,\infty), H)$, with $H = \{\phi \in \mathcal{D}'(\mathbb{R}^2),\ \nabla\phi \in L^2(\mathbb{R}^2)\}$, unique up to an additive constant.

Since u satisfies $\nabla \cdot u = 0$, this proposition guarantees that u belongs to $L^1_{\rm loc}([0,\infty), H_{\rm div}(\mathbb{R}^2))$. For such velocities, this allows us to define n as a weak solution of (2.12) in the sense of (3.6). Therefore, it is meaningful to look for solutions with discontinuous densities. Of course, we have not shown the actual existence of such solutions, which will be the subject of future work. Now, we recall the following classical trace property [14]:

LEMMA 3.6. *Let C be a regular orientable curve of $\mathbb{R}^2$. Then, the mapping $\gamma_N : v \to (v \cdot N)|_C$ (with N the unit normal vector to C) defined on $\mathcal{D}(\mathbb{R}^2)$ can be extended by continuity to a linear and continuous mapping, still denoted by γ_N, from $H_{div}(\mathbb{R}^2)$ into $H^{-1/2}(C)$.*

We are now ready to determine the conditions that f must fulfill for n to be a weak solution. We have

PROPOSITION 3.7. *Let u belong to $L^1_{loc}([0,\infty), H_{div}(\mathbb{R}^2))$. A function n defined by (3.5) is a weak solution to (2.12) if and only if f is a smooth solution to the equation*

$$\partial_t f = (u \cdot N)\left(1 + (\partial_{x_1} f)^2\right)^{1/2}, \quad (x_1, t) \in \mathbb{R} \times [0,\infty)\,, \tag{3.7}$$

where N is the unit normal vector to the curve of discontinuity $C(t)$ (pointing towards $x_2 > 0$) and $(u \cdot N)$ is the trace along $C(t)$ as defined by Lemma 3.6. We can write $(u \cdot N)\left(1 + (\partial_{x_1} f)^2\right)^{1/2} = [u_2 - u_1 \partial_{x_1} f]\,|_C$, where the index C indicates that this quantity is the common limit of the bracket as $x_2 \to f(x_1,t)$ from above and below.

Proof. We insert the expression of n in (3.6). We get

$$0 = \underline{n} \int_{x_2 < f,\, t \geq 0} (\partial_t \varphi + \nabla \cdot (u\varphi))\ dx\, dt + \overline{n} \int_{x_2 > f,\, t \geq 0} (\partial_t \varphi + \nabla \cdot (u\varphi))\ dx\, dt\,.$$

Since φ is compactly supported, we have $\int_{\mathbb{R}^2 \times [0,\infty)} (\partial_t \varphi + \nabla \cdot (u\varphi))\ dx\, dt = 0$. We regard φ as compactly supported in $\mathbb{R}^2 \times (0,\infty)$ since the treatment of the initial condition at $t = 0$ is standard. We deduce that

$$0 = (\underline{n} - \overline{n}) \int_{x_2 < f,\, t \geq 0} (\partial_t \varphi + \nabla \cdot (u\varphi))\ dx\, dt\,. \tag{3.8}$$

In order to apply the Green formula, we use Lemma 3.6. We define the surface $\Sigma = \{(x,t) \in \mathbb{R}^2 \times [0,\infty),\ x \in C(t)\}$ and the open sets $\mathcal{O}(t) = \{x \in \mathbb{R}^2,\quad x_2 < f(x_1,t)\}$ and $\Omega = \{(x,t) \in \mathbb{R}^2 \times [0,\infty),\ x \in \mathcal{O}(t)\}$. Let $\tilde{N} = (\tilde{N}_1, \tilde{N}_2, \tilde{N}_t)$ be the outgoing unit normal to Ω at (x,t) of Σ and $\tilde{N}_x = (\tilde{N}_1, \tilde{N}_2)$. Thanks to Lemma 3.6, we can apply the Green formula and get:

$$\int_\Omega (\partial_t \varphi + \nabla \cdot (u\varphi))\ dx\, dt = \int_\Sigma \varphi \left(\tilde{N}_t + u \cdot \tilde{N}_x\right) d\Sigma(x,t)\,,$$

where the integrals on Σ should be understood as the duality $L^\infty([0,\infty), H^{1/2}(C(t)))$ against $L^1([0,\infty), H^{-1/2}(C(t)))$. Now, we have $\tilde{N} d\Sigma(x,t) = (-\partial_{x_1} f,\ 1,\ -\partial_t f)\, dx_1\, dt$

which implies $\tilde{N}_x d\Sigma(x,t) = (1+(\partial_{x_1} f)^2)^{1/2} N\, dx_1\, dt$. Assuming that $\underline{n} \neq \overline{n}$, (3.8) gives

$$\int_{\mathbb{R}\times[0,\infty)} \varphi \left((u\cdot N)\left(1+(\partial_{x_1} f)^2\right)^{1/2} - \partial_t f \right) dx_1\, dt = 0\,, \tag{3.9}$$

Since (3.9) has to be verified for all test functions φ, we deduce (3.7). □

Then, the striation model (2.10) (2.13) for weak solutions can be written:

$$\partial_t f = [\partial_{x_2}\phi\, \partial_{x_1} f + \partial_{x_1}\phi]\,|_{C(t)}\,, \tag{3.10}$$

$$-\nabla\cdot((\underline{n}\chi_f + \overline{n}(1-\chi_f))(\nabla\phi - u_n \times B)) = 0\,, \tag{3.11}$$

with $\chi_f = 1$ if $x_2 < f(x_1,t)$ and $\chi_f = 0$ otherwise.

We now turn to the stability analysis of the striation model with discontinuous initial density. A steady state of this model is given by $f^0 = 0$, $\nabla\phi^0 = (0,-V)$, $u_n = (V,U)$. We define the small perturbations of order ε as $f = \varepsilon f^1$, $\phi = \phi^0 + \varepsilon\phi^1$, with $\varepsilon \ll 1$. We introduce this Ansatz in (3.10), (3.11) and keep only the terms of order ε. We get

$$\left(\partial_t f^1 + V\partial_{x_1} f^1 - \partial_{x_1}\phi^1\right)|_{(x_1,0,t)} = 0\,, \tag{3.12}$$

$$-\nabla\cdot(n^0\nabla\phi^1) = -U\lim_{\varepsilon\to 0}\varepsilon^{-1}\partial_{x_1}(\underline{n}\chi_{(\varepsilon f^1)} + \overline{n}(1-\chi_{(\varepsilon f^1)}))\,. \tag{3.13}$$

where $n^0 = \underline{n}\chi_0 + \overline{n}(1-\chi_0)$ is the unperturbed density profile. A simple computation leads to $\partial_{x_1}\chi_{(\varepsilon f)} = \varepsilon(\partial_{x_1} f)\delta_{x_2=0} + O(\varepsilon^2)$, where the distribution $g(x_1)\delta_{x_2=0}$ is defined through the relation $\langle g(x_1)\delta_{x_2=0},\varphi\rangle = \int_{\mathbb{R}}\varphi(x_1,0)g(x_1)\,dx_1$ with $\varphi(x)\in C_c^\infty$. Then, (3.13) reads

$$-\nabla\cdot(n^0\nabla\phi^1) = U(\overline{n}-\underline{n})\partial_{x_1} f^1\,\delta_{x_2=0}\,. \tag{3.14}$$

Like in the exponential density profile case, we develop the solution as a plane wave in the x_1 direction: $(f^1,\phi^1) = (\bar{f},\bar{\phi}(x_2))\exp i(\xi x_1 - \omega t)$, where $\bar{f}$ and $\bar{\phi}(x_2)$ must be determined.

We introduce the plane-wave Ansatz in (3.12), (3.14), and we get

$$-i\omega\bar{f} + iV\xi\bar{f} = i\xi\bar{\phi}(0)\,, \tag{3.15}$$

$$-\left(\partial_{x_2}\left(n^0\partial_{x_2}\bar{\phi}\right) - \xi^2 n^0\bar{\phi}\right) = U(\overline{n}-\underline{n})i\xi\bar{f}\delta_{x_2=0}\,. \tag{3.16}$$

If we solve (3.16) away from the point $x_2 = 0$ and look for a bounded solution when $|x_2|\to\infty$, we find $\bar{\phi}(x_2) = \bar{\phi}(0)e^{-|\xi||x_2|}$. Then, in the distributional sense on $\mathbb{R}$, we have:

$$-\left(\partial_{x_2}\left(n^0\partial_{x_2}\bar{\phi}\right) - \xi^2 n^0\bar{\phi}\right) = -(\underline{n}+\overline{n})|\xi|\bar{\phi}(0)\delta_{x_2=0}\,. \tag{3.17}$$

We introduce (3.17) in (3.16) and find

$$i\xi\bar{f}\delta_{x_2=0} - \frac{\overline{n}+\underline{n}}{\overline{n}-\underline{n}}\frac{|\xi|}{U}\bar{\phi}(0)\delta_{x_2=0} = 0\,. \tag{3.18}$$

Solving for $\bar{f}$ thanks to (3.15) and inserting it into (3.18) allows us to find the dispersion relation:

$$\omega = -V\xi - i\,U\frac{\overline{n}-\underline{n}}{\overline{n}+\underline{n}}\,\xi \tag{3.19}$$

We can easily deduce the stability result:

PROPOSITION 3.8. *Let us assume that $\overline{n} > \underline{n}$. Steady-states defined by (3.5) with $f = 0$ are stable if and only $U \geq 0$. Furthermore, if $U < 0$, all wave-vectors ξ are unstable. The growth rate of the instability is given by*

$$|\Im m(\omega)| = \frac{\overline{n} - \underline{n}}{\overline{n} + \underline{n}} U |\xi| , \tag{3.20}$$

This theorem makes the formal analysis of section 3.1 more quantitative. We note that the growth rate increases linearly as a function of ξ, while it is was a constant in the exponential density case (section 3.2). This feature prevents from extending the non-linear instability theorem of [5] to the discontinuous case.

3.4. Conclusion of the stability analysis. The instability contributes to the development of smaller and smaller structures in the plasma. Quickly, the plasma becomes chaotic (see section 6). In practice, the instability saturates after reaching some level by the effects of physical dissipation mechanisms, which are not accounted for so far in the model. We can think of three sources of physical dissipation: (i) finite temperature effects; (ii) finite conductivity effects; (iii) turbulence effects. By remark 3.1, we have seen that finite temperature effects alone do not change the results of the stability analysis. Therefore, we must simultaneously introduce finite temperature and finite conductivity effects, i.e. we must go back to the full dynamo model (2.1)-(2.3). In section 4, we perform the stability analysis of the dynamo model and show that large wave-vector perturbations are stable. However, the level of dissipation i.e. the threshold wave-number for stability is too large to match practical observations. Therefore, in section 5, we investigate the effects of fluid turbulence.

4. Stability analysis of the dynamo model (2.1)-(2.3). This analysis can be found, in parts, in [11], [12]. We consider steady-states with exponential density profiles. Due to diffusion, discontinuous density profiles are not steady-states of the dynamo model any longer and there is no point in trying to analyze their stability. To simplify the analysis and to make it as close as that of the striation model in section 3.2, we still consider a uniform magnetic field pointing in the x_3-direction and we suppose that u_n is orthogonal to B. All unknowns are independent of x_3 and vectors are contained in the plane (x_1, x_2). We assume that ν_e and ν_i are constants.

The steady state is given by

$$\begin{aligned}
&n^0 = N \exp(y/\lambda) , \quad u_n = (V, U) , \quad h^0 = \left((\nu_i + \nu_e)U - 2\eta\lambda^{-1}\right) \hat{x}_1 , \\
&u_i^0 = \left\{\kappa\nu_e(U - 2\eta(\nu_i + \nu_e)^{-1}\lambda^{-1}) + V\right\} \hat{x}_1 , \\
&u_e^0 = \left\{-\kappa\nu_i(U - 2\eta(\nu_i + \nu_e)^{-1}\lambda^{-1}) + V\right\} \hat{x}_1 , \\
&\nabla\phi^0 = \begin{pmatrix} -\kappa^2\nu_i\nu_e(U - 2\eta(\nu_i + \nu_e)^{-1}\lambda^{-1}) \\ -\kappa(\nu_e - \nu_i)(U - \eta(\nu_i + \nu_e)^{-1}\lambda^{-1}) - V \end{pmatrix} ,
\end{aligned}$$

We proceed to the linear stability analysis as in section 3.2. We introduce the perturbation $n = n^0(1 + \varepsilon n^1 + O(\varepsilon^2))$, $u_{i,e} = u_{i,e}^0 + \varepsilon u_{i,e}^1 + O(\varepsilon^2)$ and $\phi = \phi^0 + \varepsilon\phi^1 + O(\varepsilon^2)$ in the dynamo model (2.1)-(2.3). We only keep order ε terms and develop the solution as a plane wave according to the same Ansatz as in section 3.2. Let us define:

$$\begin{aligned}
&\mu_-^H = \mu_i^H - \mu_e^H , \quad \mu_+^H = \mu_i^H + \mu_e^H , \quad \mu_-^P = \mu_i^P - \mu_e^P , \quad \mu_+^P = \mu_i^P + \mu_e^P , \\
&X = \xi_1\mu_i^H - \xi_2\mu_i^P , \quad Y = \xi_1\mu_-^H - \xi_2\mu_+^P , \quad Z = \xi_1\mu_+^H - \xi_2\mu_-^P , \\
&A_X = \mu_i^P|\xi|^2 + iX , \quad A_Y = \mu_+^P|\xi|^2 + iY , \quad A_Z = \mu_-^P|\xi|^2 + iZ .
\end{aligned}$$

Then, we get the dispersion relation

$$\omega = \frac{\overline{A_Y}}{|U|^2|A_Y|^2}\left(\xi_1 u^0_{ix} - i\frac{\kappa\eta}{\lambda}A_X|U|A_Y - \xi_1(h^0_x)|U|A_X + i\frac{\kappa\eta}{\lambda}A_X|U|A_Z\right). \tag{4.1}$$

The expression of $\Im m(\omega)$ may be simplified as

$$\begin{aligned}\Im m(\omega) = \quad & \frac{\mu_i^P\mu_e^P}{|A_Y|^2}\left\{-\frac{\sigma(\nu_i+\nu_e)^2}{\nu_i\nu_e}\xi_1^2|\xi|^2 - \right. \\ & \left. -\frac{2\kappa\eta}{\lambda|U||A_Y|^2}\left[\mu_+^P|\xi|^6 + \mu_+^P|\xi|^2(\xi_2^2-\xi_1^2) - 2\mu_-^H|\xi|^2\xi_1\xi_2\right]\right\}.\end{aligned} \tag{4.2}$$

where $\sigma = U/|U|$ refers to the sign of U. Letting $\alpha = \kappa^2\nu_i^2 + 1$ and $\beta = \kappa^2\nu_e^2 + 1$, we can write

$$\frac{\mu_i^P\mu_e^P}{|A_Y|^2} = \frac{\nu_i\nu_e}{(\nu_i+\nu_e)^2}\Theta_0, \tag{4.3}$$

with

$$\Theta_0 = \frac{\alpha\beta}{((\nu_i\nu_e\kappa^2+1)^2|\xi|^4 + (\kappa(\nu_i-\nu_e)\xi_1 - (\nu_i\nu_e\kappa^2+1)\xi_2)^2)} > 0, \tag{4.4}$$

If $\kappa \to 0$, the dynamo model reduces to the striation model with non-zero temperature, which has the same dispersion relation (3.4) as the striation model with zero-temperature (see remark 3.1). A close inspection of (4.2) shows that, in the limit $\kappa \to 0$ we actually recover the imaginary part of (3.4). On the other hand, if we let the temperature go to zero (i.e. $\eta \to 0$) in (4.2) while keeping κ finite, we find $\Im m(\omega) = -\Theta_0\sigma\xi_1^2|\xi|^2$. Again, the stability conditions for this model are the same as those of the striation model, i.e. the model is unstable for all wave-vectors if $\sigma < 0$ and stable otherwise. Therefore, for the model to exhibit a stable range of wave-vectors, we need at the same time a finite conductivity and a finite temperature. We now show that this is indeed the case.

PROPOSITION 4.1. *Suppose that $\eta > 0$ and $\kappa > 0$. Then, there exists $R_0(\eta,\kappa) \geq 0$, such that the dynamo model (2.1)-(2.3) linearized about the above-defined steady-states is stable for all wave-vectors ξ such that $|\xi| \geq R_0(\eta,\kappa)$.*

Proof. We introduce polar coordinates $\xi_1 = r\cos\theta$ and $\xi_2 = r\sin\theta$. The study of $\Im m(\omega)$ reduces to the study of the function

$$f(\xi) = -br^4(r^2 + \Sigma(\theta)), \quad \Sigma(\theta) := ab^{-1}\cos^2\theta - \cos 2\theta - b^{-1}(c/2)\sin 2\theta \tag{4.5}$$

where

$$a = -\sigma\Theta_0, \quad b = \frac{\nu_i\nu_e}{(\nu_i+\nu_e)^2}\Theta_0\frac{2\kappa\eta}{\lambda|U||A_Y|^2}\mu_+^P, \quad c = 2\mu_-^H.$$

We remark that Σ is a bounded function of θ. Denote by $\Sigma_0 = \min(0, \min_\theta \Sigma)$ and $R_0 = \Sigma_0^{1/2}$. Then, for wave-vectors ξ such that $r = |\xi| \geq R_0$, the dynamo model is stable. ∎

The fact that the model is stable apart from a bounded region of wave-vectors can be seen as a favorable feature. Indeed, in such a case, small wave-vector (i.e. long wave-length) perturbations first grow exponentially due to the instability, but also undergo a mode cascade towards higher wave-numbers due to nonlinearity. Once the

wave-vectors are large enough to reach the stability region, they are damped by the dissipation. We therefore expect that only structures of typical size R_0^{-1} will remain for long times.

However, the values of the physical parameters in the dynamo model are too small to ensure a viable stabilization process. Indeed, we see on (2.4) that $\kappa^2\eta \sim 10^{-7}$. Since b is of the order of $\kappa^2\eta$ (if $|\xi| \neq 0$) and appears at the denominator of (4.5), the minimal value of Σ is negative and large. Therefore, the radius R_0 beyond which wave-vectors become stable is large of order $O((\kappa^2\eta)^{-1/2})$. This is too large compared with the observations (see e.g. [11], [12]). Therefore, another dissipation mechanism must be present. In this paper, we postulate that the turbulence of the plasma induced by the instability modifies the dissipation constants in a way similar to what is believed to happen in fluid mechanics (see e.g. [30] and references therein). To make this assumption more quantitative, in the next section, we develop a statistical approach to turbulence adapted to the striation model.

5. A 'turbulent' striation model.

5.1. Derivation of the 'turbulent' striation model. To produce this new model, we follow the statistical approach to turbulence [30] (see also [26] for an application to MHD). We suppose that the unknowns (n, u, ϕ, h) in the striation model (2.10), (2.13) are random variables representing the possible realizations of the flow. Any of these quantities a can be decomposed according to $a = \bar{a} + a'$ where $\bar{a}$ is its mean value and a' is a random fluctuation about this average. Since the randomness concerns the realization of the flow, the mean value operator commutes with the space and time derivatives. Therefore, we have:

$$\overline{(\bar{a})} = \bar{a}\,, \quad \overline{a'} = 0\,, \quad \nabla a = \nabla\bar{a} + \nabla a'\,, \quad \partial_t a = \partial_t\bar{a} + \partial_t a'\,.$$

If b is a non-fluctuating quantity, we have $\overline{ba} = b\bar{a}$ and for two random quantities a and b, $\overline{ab} \neq \bar{a}\bar{b}$ unless they are statistically independent. However, we note that $\overline{a\bar{b}} = \bar{a}\bar{b}$.

We assume that u_n and ν are non-fluctuating quantities. Under this assumption, by averaging the striation model (2.10)-(2.13), we obtain:

$$\partial_t\bar{n} + \nabla\cdot(\overline{nu}) = 0\,, \quad \bar{u} = -\nabla\bar{\phi}\,, \tag{5.1}$$

$$\nabla\cdot(\overline{nh}) = 0\,, \quad \bar{h} = -\nu(\bar{u} - u_n)\times B\,. \tag{5.2}$$

We can write $\overline{nu} = \bar{n}\bar{u} + \overline{n'u'}$ with $\overline{n'u'} \neq 0$, since n' and u' are in general not independent random variables. In a same way, we have $\overline{nh} = -\nu(\bar{n}\bar{u} + \overline{n'u'} - \bar{n}u_n)\times B \neq \bar{n}\bar{h}$.

To close the model, we need a prescription for the correlation $\overline{n'u'}$ as a function of the mean quantities. As in fluid turbulence (see e.g. [30]), we model this correlation by means of a diffusion term acting on the density, i.e.

$$\overline{n'u'} = -D\nabla\bar{n}\,, \tag{5.3}$$

where $D > 0$ is a diffusion coefficient. The use of this Ansatz can be formally justified by invoking Kesten-Papanicolaou's theorem [25] (see also [30] for a review and [33] for a related result). For simplicity, we assume that D is a constant. Under this assumption, and noting that $\nabla\cdot(\overline{n'u'}\times B) = -D\nabla\cdot(\nabla n\times B) = 0$, system (5.1)-(5.1) reduces to the following (turbulent striation) model (dropping the bars):

$$\partial_t n + \nabla\cdot(nu) - \nabla\cdot(D\nabla n) = 0\,, \quad u = -\nabla\phi\times B\,, \tag{5.4}$$

$$\nabla\cdot(nh) = 0\,, \quad h = \nu\left(-\nabla\phi + u_n\times B\right)\,. \tag{5.5}$$

The difficulty is now to find the correct value for the diffusion coefficient D. For this purpose, we again proceed to a stability analysis, in a similar fashion as what was done in sections 3.2 and 4.

5.2. Stability analysis of the turbulent striation model. We again choose a steady state characterized by an exponential density profile and uniform neutral wind $u_n = (V, U)$ and electric field. The unperturbed state is defined by $n_0 = Ne^{x_2/\lambda}$, $u_0 = (V, 1/\lambda) = (-\partial_{x_2}\phi_0, \partial_{x_1}\phi_0)$. We introduce $\bar{D}$ such that $D = |U|\lambda\bar{D}$. We proceed as in sections 3.2 and 4 and we get the following imaginary part of the dispersion relation (with $\sigma = \text{sign}(U)$):

$$\Im m(\omega) = \frac{\mathcal{N}}{\mathcal{D}}\ , \quad \mathcal{N} = -\bar{D}|\xi|^2(|\xi|^4 + \xi_2^2) - (\sigma - \bar{D})\xi_1^2|\xi|^2\ , \quad \mathcal{D} = |\xi|^4 + \xi_2^2\,, \tag{5.6}$$

Since $\mathcal{D} \geq 0$, we just have to discuss the sign of $\mathcal{N}$. We introduce the polar coordinates $\xi_1 = r\cos\theta$ and $\xi_2 = r\sin\theta$. Then, $\mathcal{N} = -\bar{D}r^4(r^2 + \sin^2\theta - (1 - \sigma\bar{D}^{-1})\cos^2\theta)$. The domain $\mathcal{I}$ defined in polar coordinates by $r \leq r(\theta) := \{(1 - \sigma\bar{D}^{-1})\cos^2\theta - \sin^2\theta\}^{1/2}$ (for all θ such that the expression inside the square root is positive) characterizes the (bounded) instability domain. We can summarize the results in the following

PROPOSITION 5.1. *(i) If $\sigma = 1$ (stable case for the original striation model) and $\bar{D} < 1$, the turbulent striation model (5.4), (5.5) linearized about the above defined stationary states is stable.*
(ii) If ($\sigma = 1$ and $\bar{D} > 1$) or $\sigma = -1$, the turbulent striation model is unstable for wave-vectors lying in the instability domain $\mathcal{I}$. $\mathcal{I}$ is bounded and contained in the ball centered at the origin and of radius $(1 - \sigma\bar{D}^{-1})^{1/2}$.

We note this strange feature that adding too large a diffusion can destabilize the striation model in the case where the unperturbed striation model is stable (case $\sigma = 1$ and $\bar{D} > 1$).

Thanks to this stability result, we can return to the problem of finding the value for D. Suppose that we know (from experimental observations for instance) that no structures finer than a certain scale ℓ can persist. This means that all perturbations with a wavelength less than ℓ are stable (i.e. are damped by dissipation), or equivalently, that all wave-vectors ξ larger than $1/\ell$ lie in the stability domain. To ensure this property, it is enough to have $1/\ell > (1 + \bar{D}^{-1})^{1/2}$ (we take $\sigma = -1$ because in practice, there are always regions where the density gradient and the neutral wind have configurations which trigger the instability, see e.g. the numerical results in section 6). This condition translates into $\bar{D} \geq \ell^2(1 - \ell^2)^{-1}$. In practice, it is legitimate to assume that $\ell \ll 1$ (because the typical size of the ultimate permanent structures is far smaller than the typical size of the observation domain). Going back to the unscaled value of the diffusion constant D, we get

$$D \gtrapprox \ell^2\lambda|U|\,. \tag{5.7}$$

In the next section, we present numerical simulations which display the relation between the typical size of the persisting structures triggered by the instability and the value of this diffusion coefficient.

6. Numerical experiments. In this section, we present some numerical simulations of the striation model (2.10), (2.13) and of the turbulent striation model (5.4), (5.5). The elliptic equation (2.13) or (5.5) is discretized by a conservative finite difference method. The plasma velocity is computed by means of finite differences applied to the second equation of (2.10) or (5.4) on staggered grids. The transport equation

(first equation of (2.10) or (5.4)) is discretized thanks to a classical TVD-scheme [15], [40], [28]. In order to deal with steep density gradients, the diffusion operator in (5.4) is implicitly discretized and we make use of a Strang splitting for the overall time discretization of this equation. A preconditioned gradient method [38] is applied to solve the linear systems resulting from the discretization of the elliptic equation (2.13) or (5.5) and from the implicit discretization of the diffusion equation (5.4).

Our first test problem is intended to mimic that of [42]. The initial density is a random perturbation of a uniform density in the x_1-direction with a Gaussian profile in the x_2-direction (cf FIG. 6.1). The neutral wind u_n is directed along the x_2-axis and has a value of 45 ms^{-1}. Different mesh sizes listed at Table 6.1 are considered.

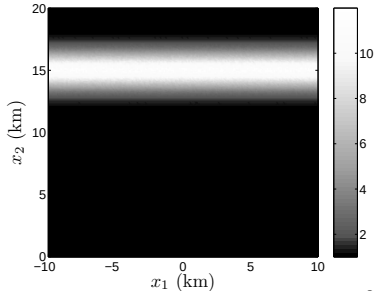

FIG. 6.1. *Initial plasma density (m^{-3})*

	Nb. of cells	Δ_x, Δ_y (m)
Mesh 1	200×200	$0.1 \quad 10^3$
Mesh 2	400×400	$0.05 \quad 10^3$
Mesh 3	800×800	$0.025\,10^3$

TABLE 6.1
Number of cells and mesh sizes

When the turbulent striation model is considered, the diffusion length ℓ (which sets the value of the diffusion coefficient through (5.7)) is equal to $0.1\,10^3$ m (a scale resolved by all mesh steps). In practice, its value should be prescribed by comparing with experimental measurements (see for instance [6]). However, our purpose here is towards qualitative rather than quantitative results.

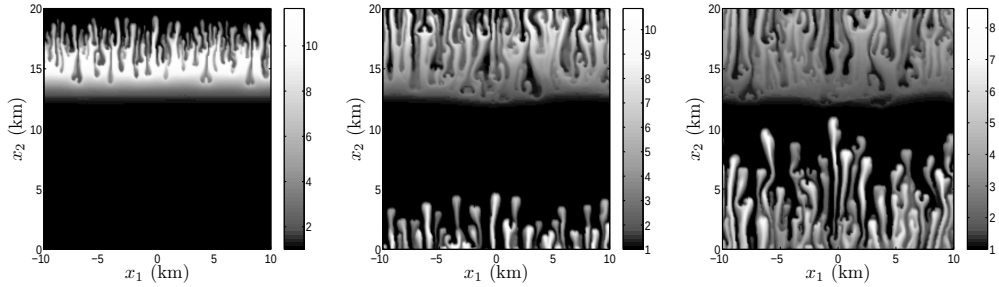

(a) t = 196 s. (b) t = 392 s. (c) t = 588 s.

FIG. 6.2. *Time evolution of the electronic density computed with the striation model (mesh 1).*

We first consider the original striation model (2.10), (2.13). Figure 6.2 displays the time evolution of the electron density as a function of the 2-dimensional coordinate x. Periodic boundary conditions are used. We see that the upper side (with respect to the orientation of the figure) of the density gradient is unstable, while the lower side is stable. The instability produces finger-like structures which rise in the positive x_2-direction and eventually (by periodicity) appear as originating from the lower boundary. In the figure 6.3 we represent the electronic density computed on the different meshes (see Table 6.1) at time $t = 804$ s. The mesh-size is divided by a factor 2 from FIG. (a) to FIG. (b) and from FIG. (b) to FIG. (c). One can notice that the number of persisting structures grows with the number of cells while their typical size decreases with the mesh-size. This remark can be made more quantitative on

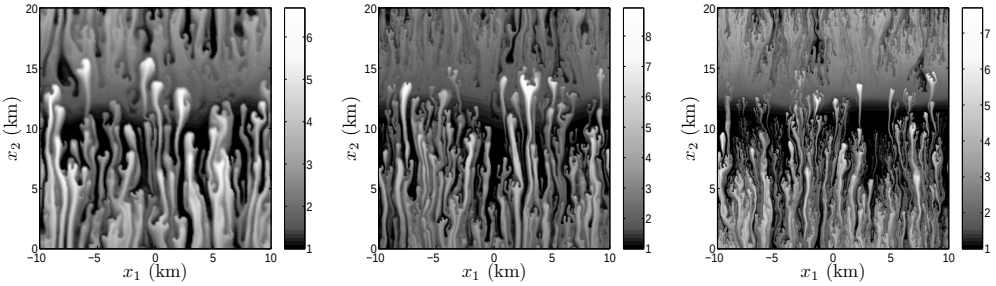

(a) Mesh 1 (200 × 200). (b) Mesh 2 (400 × 400). (c) Mesh 3 (800 × 800).

FIG. 6.3. *Electronic density after 804 sec, with the striation model.*

Figure 6.6 where the spectral density associated with the plasma density is displayed for the coarsest and finest meshes (dashed line curves). *We recall that the spectral density of a function $f(x)$ is defined by $|\widehat{f}(\xi)|$, where $\widehat{f}(\xi)$ is the Fourier transform of f,* and provides a quantitative measure of the contribution of any given Fourier mode of (spatial) frequency ξ. We can see that high frequency modes (corresponding to space scales ranging from 2 to 5 times the value of ℓ) have a significantly larger contribution when the finest mesh is used. Correspondingly, on Figure 6.3, we notice that the structures are all the more tinier that the mesh is finer.

This behavior can be related with the instability of the model. Indeed, numerical diffusion is the only damping mechanism and the numerical diffusivity is proportional to the mesh size [15], [40], [28]. According to the stability analysis in section 5.2, the diffusive striation model becomes stable for wave-vectors of the order of $1/\sqrt{D}$, which is proportional to $1/\sqrt{\Delta x}$. Therefore, the size of the typical persisting structures must be divided by a factor $\sqrt{2}$ each time the mesh-size is divided by 2. This is roughly speaking what we observe *on Figure 6.5 where the variations of the density, with respect to the first coordinate, are plotted. The calculation carried out on the coarsest mesh (plain line of* FIG. *6.5(a)) exhibits 5 to 6 main structures (area where the density varies significantly) in the last quarter of the x_1 range. In the same interval approximately 14 main structures are counted for the density profile computed with the finest grid (plain line of* FIG. *6.5(b)). Note that small patterns can exist in addition to this persisting structures. Indeed the counting of the local maxima number gives 7 and more than 20 for meshes 1 and 3 respectively. The same ratio is recovered from figure 6.7 where, the time evolution of the number of local maxima is displayed. For long time evolution (greater than 600 sec.) the number of local maxima can be estimated has 25 for the coarsest mesh and 85 for the finest one. These results confirm the mesh dependence of the density computed thanks to the striation model.*

We next consider the turbulent striation model (5.4), (5.5). Figure 6.4 demonstrates the stability brought by the diffusion : the number and size of the structures remain almost the same when the mesh resolution increases. *The dashed line curves of figure 6.5 are associated to density profiles carried out on the coarsest and the finest mesh respectively. The small patterns observed on results computed thanks to the classical striation model (plain line curves) no more exist. Moreover, the number of local maxima (6 for mesh 1, 7 for the mesh 3) observed on density profiles plotted in figure 6.5 are quite independent of the grid resolution. The same invariance with respect to the grid resolution stands out the analysis of the number of local maxima*

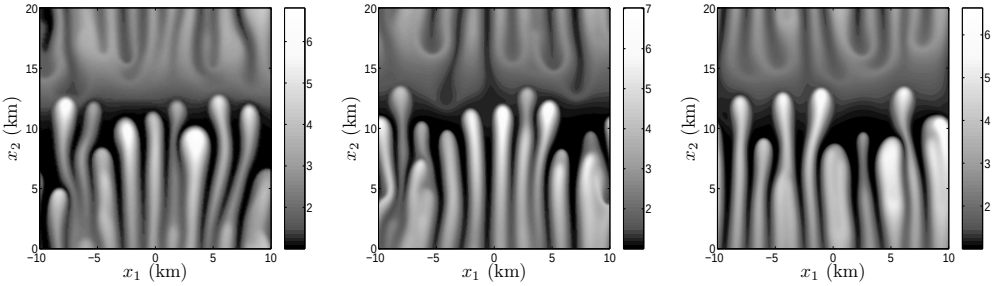

(a) Mesh 1 (200 × 200). (b) Mesh 2 (400 × 400). (c) Mesh 3 (800 × 800).

FIG. 6.4. *Electronic density after 804 sec, with the turbulent striation model.*

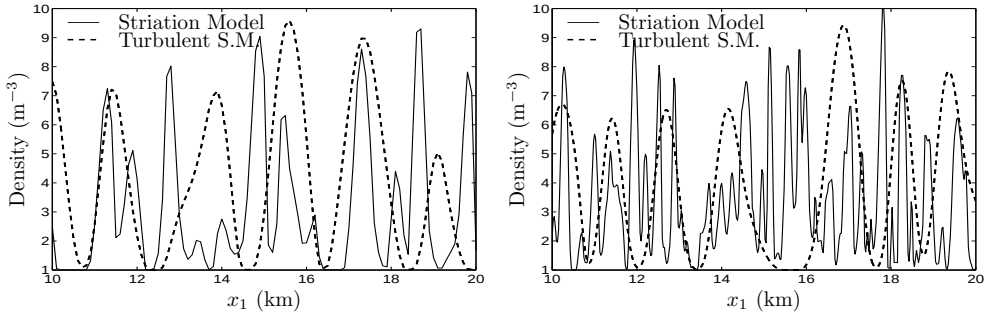

(a) Mesh 1 (second half of the x_1 range). (b) Mesh 3 (second half of the x_1 range).

FIG. 6.5. *Electronic density profile along the x_1 axis. The curves are plotted for x_2 = 2 km and t= 392 s.*

*evolution (*FIG. *6.7). This quantity remains almost constant and equal to 9 when the mesh size varies. This is a main difference with the results obtained thanks to the striation model.* The spectral densities computed with the turbulent striation model are displayed on Figure 6.6. The diffusion damps the high frequency modes out and the two curves are very similar whatever space scales are considered, by contrast with the behavior of the original striation model.

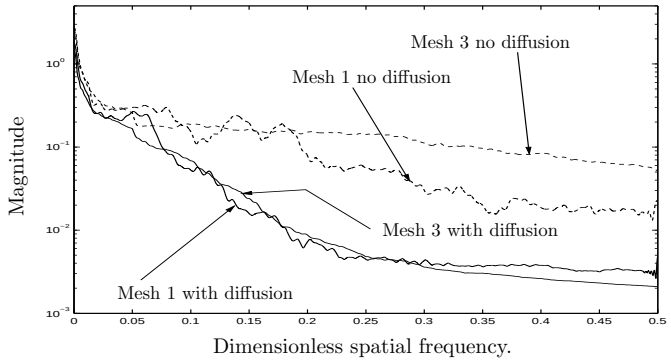

FIG. 6.6. *Spectral density associated with the plasma density computed on the coarsest and the finest meshes of table 6.1. The vertical axis represents the magnitude of the mode, the horizontal axis is the dimensionless spatial frequency, i.e. the ratio of the spatial frequency and ℓ^{-1}, ℓ being the parameter introduced in equation* (5.7)*, the value of which is* $0.1\,10^3$ *m.*

Plotter le nombre de minima ou de maxima en fonction de t pour illustrer que la diffusion ne contribue pas a aggréger les structures avec le temps.

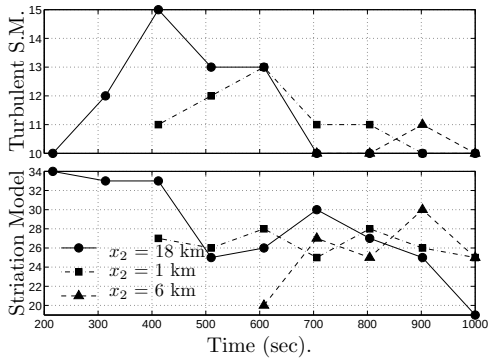

(a) Mesh 1 (200 × 200).

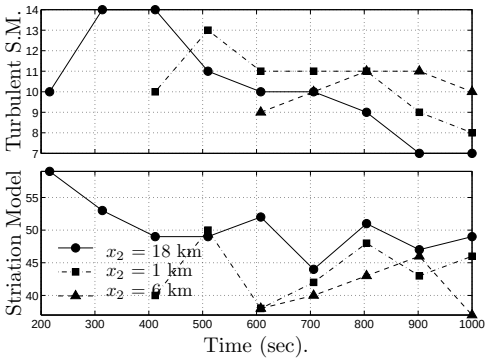

(b) Mesh 2 (400 × 400).

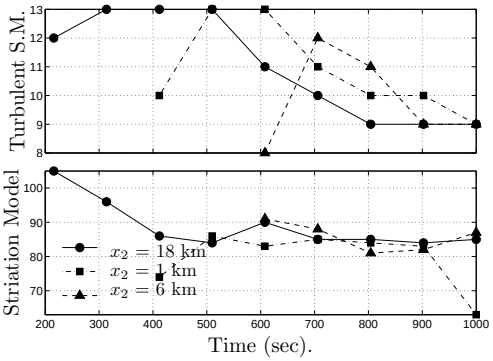

(c) Mesh 3 (800 × 800).

FIG. 6.7. *Time evolution of the density profile monotony.*

The number of local maxima is computed as half the number of sign changes in the density derivative. This sum is performed for density profiles varying with the first coordinate at different values for x_2 (18, 1 and 6 kilometers for respectively the curves with circles, squares and triangles). The top pictures display this quantity for the Turbulent striation model (Turbulent S.M.) the bottom ones being dedicated to the classical model.

Note that the characteristic size of the striations observed on figures 6.4 and 6.5 amounts to a few kilometers, which suits well with the experimental observations.

The second simulation is aimed at illustrating the results of the stability analysis developped in the discontinuous density profile framework (see section 3.3). To this purpose, we consider a similar set of simulation parameters as above, excepting from the initial density and the neutral wind. The initial density consists in a plasma bubble (density equal to one) in a quasi vaccuum media (density almost vanishing). This initial data is perturbated by a random noise. The neutral wind is oriented along the x_1 axis, its speed is set to 100 $m.s^{-1}$. Simulations performed on the mesh 2 (table 6.1) with the classical striation model are displayed on figures 6.8(a), 6.8(b) and 6.8(c) respectively at time $t = 0$, 281.4 and 562.8 seconds. The plasma bubble is set into motion by the neutral wind and since periodic boundary conditions are used, the bubble seems to go out of the domain at the right side of the frame and to re-enter the computational box at the left side. The instabity observed on the first simulation still occurs on the right side of the bubble frontier, the other side being unaffected.

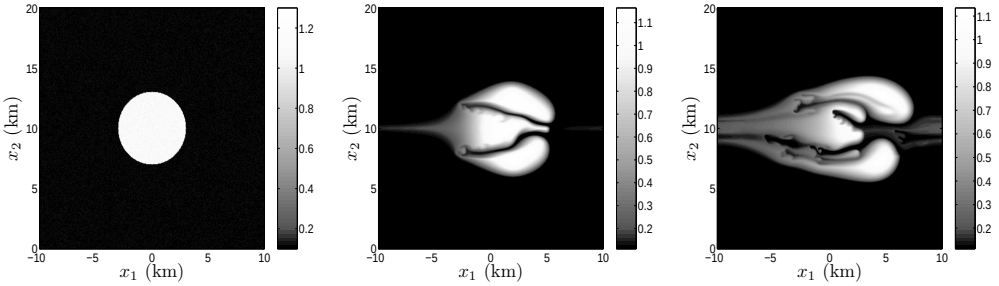

(a) Initial Density. (b) t = 281.4 s. (c) t = 562.8 s.

FIG. 6.8. *Striation model simulation with an initial discontinuous density. (simulations performed on Mesh 2).*

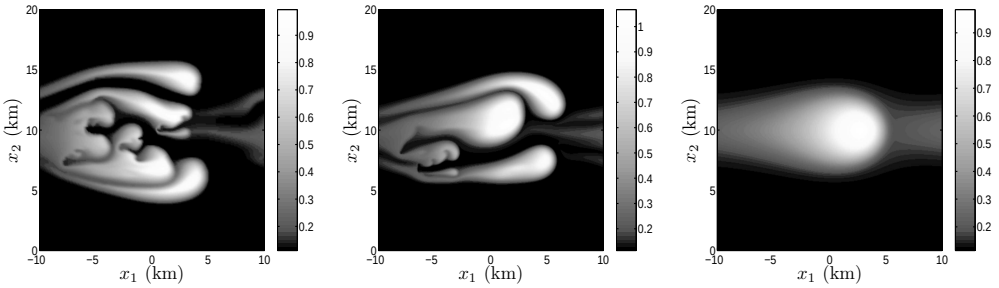

(a) Striation model on Mesh 1. (b) Turbulent SM with low diffusion. (c) Turbulent SM with high diffusion.

FIG. 6.9. *Mesh size and diffusion influence on the simulations. Simulation of the discontinous initial plasma represented on figure 6.8(a). The densities displayed correspond to t = 562.8 seconds.*

The same simulation run on mesh 1 produces the result displayed on figure 6.9(a) and shows the sensitivity of the patern created by the instability with respect to the grid resolution. The last two pictures 6.9(b) and 6.9(c) are related to calculations performed thanks to the turbulent striation model on mesh 2. The diffusion parameter used on FIG. *6.9(c) is four times as big as the one considered for 6.9(b). When comparing* FIG. *6.8(c) (without any diffusion) and* FIG. *6.9(b) we get the same conclusion as before : diffusion brings stability for small space scales, since the tiniest paterns have diseapeared from figure 6.9(b). More diffusion can also brings stability for all space scales and prevents the growth of the instability, as demonstrated by the results of figure 6.9(c)*

7. Conclusion. In this paper, we have been concerned with the modeling of ionospheric plasma instabilities. The first main point of this work was to remark that the 'striation model' allows for discontinuous solutions and that discontinuous steady-states may be unstable in a similar way as smooth ones. The second point was to propose that the turbulence induced by the instability may actually produce diffusion, in a similar way as what occurs in fluid mechanics, and that this diffusion may actually contribute to stabilize large wave-number perturbations. Following the statistical approach to turbulence, we have derived and analyzed a 'turbulent striation

model'. Numerical simulations have been produced in support to our analysis.

REFERENCES

[1] W. G. Baker, D. F. Martyn, *Electric currents in the ionosphere, I. The conductivity*, Phil. Trans. Roy. Soc. London, A246 (1953), pp. 295–305 (see also parts II et III in the same issue).

[2] J. J. Berthelier, *L'ionosphère*, in 'Environnement spatial: prévention des risques liés aux phénomènes de charge', J. P. Catani et M. Romero (eds), Cépaduès éditions, Toulouse, 1996.

[3] C. Besse, J. Claudel, P. Degond, F. Deluzet, G. Gallice, C. Tessieras, *A Model Hierarchy for Ionospheric Plasma Modeling*, to appear in Math. Models Methods Appl. Sci.

[4] C. Besse, J. Claudel, P. Degond, F. Deluzet, G. Gallice, C. Tessieras, *Numerical simulations of the ionospheric dynamo model in a non-uniform magnetic field*, in preparation.

[5] C. Besse, P. Degond, H-J. Hwang, R. Poncet, *A rigorous proof of the nonlinear gradient-drift instability in the framework of the ionospheric dynamo model*, in preparation.

[6] E. Blanc, B. Mercandelli, E. Houngninou, *Kilometric irregularities in E and F regions of the daytime equatorial ionosphere observed by a high resolution HF radar*, Geophysical Research Letters, 23 (1996), pp. 645–648.

[7] J. W. Chamberlain, D. W. Hunter, *Theory of planetary atmospheres*, Academic Press, New-York, 1987.

[8] S. Chandrasekhar, *Hydrodynamic and hydromagnetic stability*, Dover, 1981.

[9] B. Desjardins, E. Grenier, *Linear instability implies nonlinear instability for various types of viscous boundary layers*, Ann. Inst. H. Poincaré Anal. Non Linéaire, 20 (2003), pp. 87–106.

[10] J. H. Doles III, N. J. Zabuski, F. W. Perkins, *Deformation and striation of plasma clouds in the ionosphere. 3. Numerical simulations of a multilevel model with recombination chemistry*, J. Geophys. Res., 81 (1976), pp. 5987–6004.

[11] D. T. Farley, *Theory of equatorial eletrojet plasma waves, new developments and current status*, J. Atm. Terr. Phys., 47 (1985), pp. 729–744.

[12] B. G. Fejer, M. C. Kelley, *Ionospheric irregularities*, Reviews of geophysics and space physics, 18 (1980), pp. 401–454.

[13] X. Garbet, *Instabilités, turbulence et transport dans un plasma magnétisé*, Habilitation dissertation, University of Marseille, France, 2001.

[14] V. Girault, P.-A. Raviart, *Finite Element Methods for Navier Stokes Equations, Theory and Algortihms*, Springer, 1986.

[15] E. Godlewski, P. A. Raviart, *Numerical Approximation of Hyperbolic Systems of Conservation Laws*, Springer, 1996.

[16] E. Grenier , *On the nonlinear instability of Euler and Prandtl equations*, Comm. Pure Appl. Math., 53 (2000), pp. 1067–1091.

[17] C.Grimault, *Caractérisation des canaux de propagation satellite-Terre SHF et EHF en présence de plasma post-nucléaire*, PhD Dissertation, University of Rennes, France, 1995.

[18] Y. Guo, W. Strauss, *Nonlinear instability of double-humped equilibria*, Ann. Inst. H. Poincaré Anal. Non Linéaire, 12 (1995), pp. 339–352.

[19] J. K. Hargreaves, *The solar-terrestrial environment*, Cambridge University Press, Cambridge, 1992.

[20] A. M. Hamza, J. P. St. Maurice, *A fully self-consistent fluid theory of anomalous transport in Farley-Buneman turbulence*, J. Geophys. Res., 100 (1995), pp. 9653–9668.

[21] A. M. Hamza, J. P. St. Maurice, *A turbulent theoretical framework for the study of current-driven E region irregularities at high latitudes: basic derivation and application to gradient-free situations*, J. Geophys. Res., 98 (1993), pp. 11587–11599.

[22] H. J. Hwang, Y. Guo, *On the dynamical Rayleigh-Taylor instability*, Arch. Ration. Mech. Anal., 167 (2003), pp. 235–253.

[23] M. J. Keskinen, *Nonlinear theory of the $E \times B$ instability with an inhomogeneous electric field*, J. Geophys. Res., 89 (1984), pp. 3913–3920.

[24] M. J. Keskinen, S. L. Ossakow, B. G. Fejer, *Three-dimensional nonlinear evolution of equatorial ionospheric spread-F bubbles*, Geophys. Res. Lett., 30 (2003), p. 1855.

[25] H. Kesten, G. C. Papanicolaou, *A limit theorem for stochastic acceleration*, Comm. Math. Phys., 78 (1980), pp. 19–63.

[26] F. Krause, K. H. Rädler, *Mean-field magnetohydrodynamics and dynamo theory*, Pergamon Press.

[27] M. Lesieur, *Turbulence in fluids: stochastic and numerical modeling*, Kluwer, 1990.

[28] R. J. LeVeque, *Numerical methods for conservation laws*, Birkhaüser Verlag, 1992.
[29] S. Matsushita *On artificial geomagnetic and ionospheric storms associated with high-altitude explosions*, J. Geophys. Res., 64, (1959) pp. 1149–1161.
[30] B. Mohammadi, O. Pironneau, *Analysis of the K-Epsilon Turbulence Model*, Wiley, 1994.
[31] M. Oppenheim, N. Otani, C. Ronchi, *Saturation of the Farley-Buneman instability via nonlinear $E \times B$ drifts*, preprint.
[32] S. L. Ossakow, P. K. Chatuverdi, *Morphological Studies of Rising Equatorial Spread F Bubbles*, J. Geophys. Res., 83 (1978), pp. 2085–2090.
[33] F. Poupaud, A. Vasseur, *Classical and quantum transport in random media*, J. Math. Pures Appl., 82 (2003), pp. 711–748
[34] G. C. Reid, *The Formation of Small-Scale Irregularities in the Ionosphere*, J. Geophys. Res., 73 (1968), pp. 1627–1640.
[35] H. Rishbeth, O. K. Garriott, *Introduction to ionospheric physics*, Academic Press, 1969.
[36] C. Ronchi, R. N. Sudan, D. T. Farley, *Numerical simulations of large-scale plasma turbulence in the daytime equatorial electrojet*, J. Geophys. Res., 96 (1991), pp. 21263–21279.
[37] C. Ronchi, R. N. Sudan, P. L. Similon, *Effect of short-scale turbulence on kilometer wavelength irregularities in the equatorial electrojet*, J. Geophys. Res., 95 (1990), pp. 189–200.
[38] Youcef Saad *SPARSKIT : a basic tool kit for sparse matrix computations - Version 2*, Tech. Rep. Computer Science Department, Univ. of Minnesota, Minneapolis, MN, 1994.
[39] R. N. Sudan, J. Akinrimisi, D. T. Farley, *Generation of small scales irregularities in the equatorial electrojet*, J. Geophys. Res., 78 (1973), pp. 240.
[40] E. F. Toro, *Riemann Solvers and Numerical Methods for Fluid Dynamics*, Springer, 1999.
[41] W. White, *An overview of high-altitude nuclear wepaons phenomena*, Heart conference short course, march 1998, preprint.
[42] S. T. Zalesak, S. L. Ossakow, *Nonlinear equatorial spread F: the effect of neutral winds and background Pedersen conductivity*, J. Geophys. Res., 87 (1982), pp. 151–166.